

Original Article

**Cite this article:** Lu H, Liu R, Cheng L, Feng H, Zhang H, Wang Y, Hu R, Zhao W, Ji J, Xu Z, Yu Z, Kulhanek DK, Pandey DK, and Clift PD. Phased evolution and variation of the South Asian monsoon, and resulting weathering and surface erosion in the Himalaya–Karakoram Mountains, since late Pliocene time using data from Arabian Sea core. *Geological Magazine* <https://doi.org/10.1017/S0016756820000291>

Received: 19 September 2018

Revised: 27 October 2019





Accepted: 25 March 2020

**Keywords:**

zircon U–Pb ages; Nd–Sr isotopes; hematite content; grain size; IODP Hole U1456A; east Arabian Sea; monsoon rainfall belt

**Author for correspondence:** Huayu Lu,  
Email: [huayulu@nju.edu.cn](mailto:huayulu@nju.edu.cn)

# Phased evolution and variation of the South Asian monsoon, and resulting weathering and surface erosion in the Himalaya–Karakoram Mountains, since late Pliocene time using data from Arabian Sea core

Huayu Lu<sup>1</sup> , Ruixuan Liu<sup>1</sup>, Linhai Cheng<sup>1</sup>, Han Feng<sup>1</sup>, Hanzhi Zhang<sup>1</sup>, Yao Wang<sup>1</sup>, Rong Hu<sup>1</sup>, Wancang Zhao<sup>1,2</sup>, Junfeng Ji<sup>2</sup>, Zhaokai Xu<sup>3</sup>, Zhaojie Yu<sup>3</sup>, Denise K. Kulhanek<sup>4</sup> , Dhananjai K. Pandey<sup>5</sup>  and Peter D. Clift<sup>6</sup> 

<sup>1</sup>Key Laboratory of Coast and Island Development, Ministry of Education, School of Geography and Ocean Science, Nanjing University, Nanjing 210023, China; <sup>2</sup>Key Laboratory of Surficial Geochemistry, Ministry of Education, School of Earth Sciences and Engineering, Nanjing University, Nanjing 210023, China; <sup>3</sup>Key Laboratory of Marine Geology and Environment, Institute of Oceanology, Chinese Academy of Sciences, Qingdao 266071, China; <sup>4</sup>International Ocean Discovery Program, Texas A&M University, 1000 Discovery Drive, College 10 Station, TX 77845, USA; <sup>5</sup>Department of Marine Geophysics, National Centre for Antarctic and Ocean Research (NCAOR), Vasco da Gama, Goa 403804, India and <sup>6</sup>Department of Geology and Geophysics, Louisiana State University, Baton Rouge, LA 70803, USA

## Abstract

We investigate the phased evolution and variation of the South Asian monsoon and resulting weathering intensity and physical erosion in the Himalaya–Karakoram Mountains since late Pliocene time (*c.* 3.4 Ma) using a comprehensive approach. Neodymium and strontium isotopic compositions and single-grain zircon U–Pb age spectra reveal the sources of the deposits in the east Arabian Sea, and show a combination of sources from the Himalaya and the Karakoram–Kohistan–Ladakh Mountains, with sediments from the Indian Peninsula such as the Deccan Traps or Craton. We interpret shifts in the sediment sources to have been forced by sea-level changes that correlate with South Asian monsoon rainfall variation since late Pliocene time. We collected 908 samples from the International Ocean Discovery Program Hole U1456A, which was drilled in the east Arabian Sea. Time series of hematite content and grain size of the sediments were examined downcore. We found South Asian monsoon precipitation and weathering intensity experienced three phases from late Pliocene time. Lower monsoon precipitation, with a lower variability and strong weathering intensity, occurred during 3.4–2.4 Ma; an increased and more variable South Asian monsoon rainfall, along with strengthened but fluctuating weathering intensity, occurred at 1.8–1.1 Ma; and a reduced rainfall with lower South Asian monsoon precipitation variability and moderate weathering intensity marked the period 1.1–0.1 Ma. Maximum entropy spectral analysis and wavelet transform show that there were orbital-dominated cycles of periods *c.* 100 and *c.* 41 ka in these proxy-based time series. We propose that the monsoon, sea level, global temperature and insolation together forced the weathering and erosion in SW Asia.

## 1. Introduction

Physical erosion, climate change and tectonic deformation (rock uplift) in the Himalaya–Karakoram Mountains in SW Asia interplayed during the Cenozoic Era. The dominant forcing process may have varied over different timescales, but has not yet been determined (Thiede *et al.* 2004, 2005; Thiede & Ehlers, 2013; Clift, 2017; Schildgen *et al.* 2018). SW Asia, which has experienced rapid tectonic uplift of mountain ranges, is an ideal place to investigate these intertwined processes. Strong surface erosion and rapid basin filling during the Cenozoic Era were thought to be closely associated with large-scale mountain uplift and the origin and evolution of the monsoon (Molnar *et al.* 1993; Boos & Kuang, 2010; Clift *et al.* 2014; Botsyun *et al.* 2019; Valdes *et al.* 2019). In 2015, the International Ocean Discovery Program (IODP) Expedition 355 drilled two deep-sea cores in the Laxmi Basin in the east Arabian Sea in order to understand the interaction between Earth-surface processes and the evolution of the South Asian (summer) monsoon (SASM) (Pandey *et al.* 2015, 2016a, b). Previous studies have demonstrated that SASM variations during late Cenozoic time played a key role in controlling surface erosion and exhumation at a tectonic timescale in mountain ranges in SW Asia (e.g. Thiede *et al.* 2004, 2005; Clift *et al.* 2008; Clift & VanLaningham, 2010; Clift, 2017). IODP Expedition 355 cores can therefore provide more

evidence for understanding the interactions between tectonic uplift, monsoon evolution and physical erosion in Asia.

Regarding the SASM evolution, early palaeo-oceanographic investigations suggested that intense upwelling, which is presently linked to the monsoon, began at *c.* 8.0 Ma in the Arabian Sea (Kroon *et al.* 1991; Prell *et al.* 1992), although more recently this appears to have begun after *c.* 13 Ma (Gupta *et al.* 2015; Betzler *et al.* 2016) or even earlier (Huber & Goldner, 2012; Roe *et al.* 2016). These proxy records and modelling studies indicate strengthened wind velocity rather than an increase in monsoon precipitation, which is very important in modulating environment in SW Asia (Clift, 2017). Limited onshore work also supports an earlier, Palaeogene onset to the monsoon in East Asia (Licht *et al.* 2014; Lu *et al.* 2018). At a millennial timescale, it is well documented that the strengthened SASM intensity and increasing monsoon precipitation determined rates of surface erosion and deposition in river deltas such as the Indus River (Goodbred & Kuehl, 2000; Clift *et al.* 2008, 2014, 2019). Moreover, enhanced monsoon precipitation has generally intensified surface erosion and led to increased sedimentation rates in the marginal seas around South Asia (Colin *et al.* 1999; Thiede *et al.* 2004, 2005; Blöthe *et al.* 2014; Clift *et al.* 2014). Sediments eroded by glaciers were then reworked to the ocean and resulted in a higher sediment accumulation rate when the summer monsoon rainfall was strong during interglacial times (Molnar, 2001; Jonell *et al.* 2017). On a large spatial scale, the glacial–interglacial climate alternations might have strengthened physical erosion under imbalanced conditions of runoff, vegetation and flooding (Zhang *et al.* 2001; Lu *et al.* 2004, 2015); however, the quantitative evaluation and specific forcing mechanism of weathering intensity, surface erosion and sediment production since late Pliocene time needs to be investigated (Thiede *et al.* 2004, 2005; Thiede & Ehlers, 2013; Schildgen *et al.* 2018).

The large difference in elevation between the western Himalaya, Karakoram and associated mountain ranges and the deep-sea basins of the Arabian Sea and Bay of Bengal makes South Asia ideal for investigating climate–tectonic–erosion interactions, under the forcing of the SASM precipitation variations, during the late Cenozoic Era. The deep-sea cores drilled during IODP Expedition 355 provide a good opportunity to examine these relationships and forcing mechanisms over a number of glacial–interglacial cycles and the longer (tectonic) timescale (Li *et al.* 2018, 2019; Yu *et al.* 2019; Clift *et al.* 2019). Samples were collected from IODP Hole U1456A in this study. This core recovered a length of 365.25 m and has been dated by biostratigraphic and magnetostratigraphic methods (Pandey *et al.* 2016a, b). Over 908 samples were obtained covering the late Pliocene (*c.* 3.4 Ma) to late Pleistocene (*c.* 0.1 Ma) period; each sample spans on average 3.6 ka. Multiple proxies including grain size distribution, hematite content, uranium (U) and lead (Pb) dating of zircon, and bulk sediment neodymium (Nd) and strontium (Sr) isotopes are described in order to reconstruct and examine the relationship between erosion and monsoon rainfall since late Pliocene time at the tectonic timescale and glacial–interglacial alternations, and to isolate the associated forcing mechanism. Our study also allows us to investigate the interplay between climatic change, surface erosion and tectonic deformation.

## 2. Materials and methods

### 2.a. Sampling and dating Hole U1456A

IODP Hole U1456A (latitude, 16° 37.2855' N; longitude, 68° 50.3272' E; water depth, 3639.23 m; cored interval, 426.60 m;

recovered length, 365.25 m; Fig. 1a) lies offshore the western margin of India, *c.* 475 km from the Indian coast and *c.* 820 km from the modern mouth of the Indus River. Based on earlier provenance work, the latter is presumed to be the primary source of sediment in the drilling site, with lesser input from rivers such as the Tapti and Narmada that originate from the Indian Peninsula (Clift *et al.* 2019) (Fig. 1a; see Discussion). The studied deposits are predominantly composed of sand, silt and clay, interpreted as turbidites interbedded with biogenic carbonate (nannofossil ooze or chalk, nannofossil-rich clay or claystone) and hemipelagic muds (Fig. 2; Pandey *et al.* 2016b). A relative reduction in siliciclastic sediment content occurred at *c.* 100 m below the seafloor (mbsf) (Fig. 2), which might represent a time of reduced Indus discharge. However, this could equally reflect higher sea levels sequestering sediment on the shelf, avulsion of the fan depositional lobes away from the Laxmi Basin into the Arabian Basin, or a bloom in biogenic productivity offshore western India, diluting the clastic flux (Pandey *et al.* 2016b). The 365.25 m core was subsequently sampled at an interval of 40 cm, resulting in 908 samples obtained for grain size distribution and diffuse reflectance spectroscopy (DRS) analyses. Eight samples were picked from interglacial-era deposits, four samples were selected from glacial sediment on the basis of stable oxygen isotope analysis for Sr and Nd isotopic analyses, and eight samples were collected throughout Hole U1456A for detrital zircon U–Pb dating analysis (Fig. 2).

A high-resolution age model for this depositional sequence was constructed by linear interpolation between 23 independent age control points; these ages were obtained from biostratigraphy and magnetostratigraphic constraints (Pandey *et al.* 2016a, b), resulting in a precise timescale (Table 1, Fig. 2). The time series has an average time resolution of 3.6 ka, which is large enough to investigate the glacial–interglacial variations of monsoon, surface erosion and sediment sources. Samples used for Sr–Nd isotopic composition analysis and zircon dating are listed in Table 2.

### 2.b. Hematite content estimated by diffuse reflectance spectroscopy

Hematite is derived from ferrihydrite through dehydration and crystallization during weathering of iron-containing minerals and rocks (Deaton & Balsam, 1991), and is preferentially preserved under a warm and dry climate with oxidizing conditions. Chemical weathering and iron oxide formation were controlled by both temperature and precipitation. Because temperature remains relatively stable in subtropical SW Asia, variations of hematite contents were expected to be regulated mostly by precipitation changes over a temperature threshold (Ji *et al.* 2002; Ji, 2004; Long *et al.* 2011). Hematite content can therefore be regarded as an indicator of warm and dry climate in SW Asia.

DRS is a rapid, precise and well-established method for measuring the hematite content of sediments and/or soils, and is commonly used in both qualitative and quantitative analyses of deep-sea sediments, mineral dust deposits and soils. The obtained spectra are especially sensitive to Fe oxides and oxyhydroxides in soils and sediments (Deaton & Balsam, 1991; Ji *et al.* 2002), and the detection limit can be as low as 0.01 wt% (Balsam & Deaton, 1996). As a primary Fe oxide, hematite exhibits peaks at 565 or 575 nm in the visible (400–700 nm) diffuse reflectance spectra, which have been used as the typical spectra for determining absolute concentration of hematite (Deaton & Balsam, 1991; Ji *et al.* 2002).

The determination of hematite using DRS is mainly based on first and/or second derivatives of the reflectance spectrum

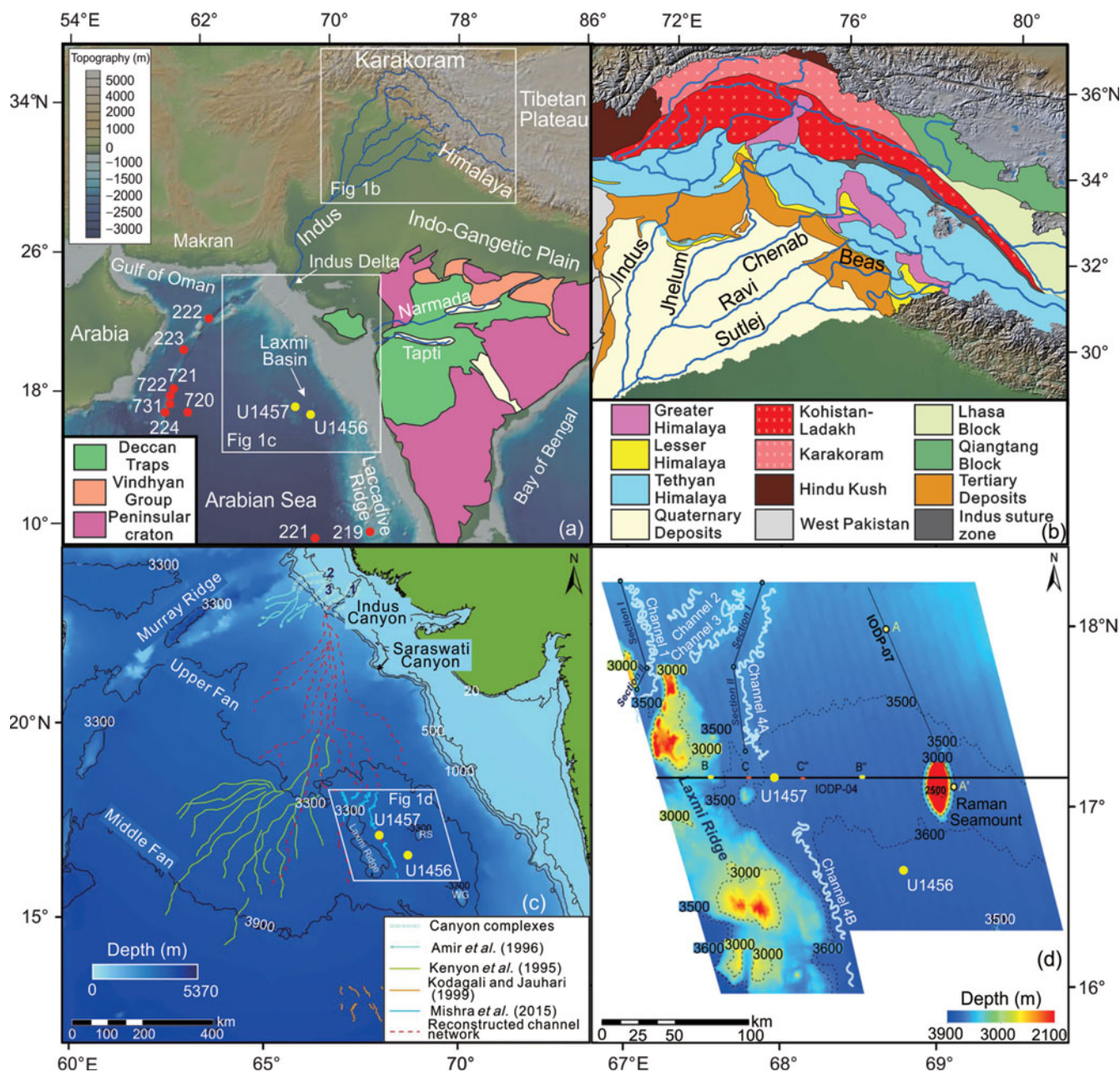


**Fig. 1.** (Colour online) Watershed of Indus River, sediment sources, IODP Expedition 355 Hole U1456A and Indus channel system at Laxmi Basin, east Arabian Sea. (a) Shaded relief of South Asia with tectonic blocks in Indian Peninsula (revised from Pandey *et al.* 2015, fig. F1). Red dots indicate previous IODP drilled sites, and yellow dots represent the IODP 355 drilled sites. (b) Tectonic blocks within the Indus River drainage basin, based on IGMA5000 (Ren, 2013) and Yin (2006). (c) Indus channel system from global bathymetry data (revised from Mishra *et al.* 2016, fig. 1b). (d) Bathymetry map of the study area showing submarine channels (revised from Mishra *et al.* 2016, fig. 2a).

(Deaton & Balsam, 1991; Scheinost, 1998). However, many studies noticed that sample reflectance can be affected by other admixed minerals (referred to as the ‘matrix effect’), which impeded the quantitative estimate of Fe oxides. Ji *et al.* (2002) introduced a calibration technique based on a series of experiments where a batch of natural samples from Hole U1456A were processed by totally removing iron oxides before adding hematite to a known concentration. A transfer function can be derived using a linear regression for determining hematite content. This method has proven to be effective in removing the matrix effect and has been used to obtain more precise concentrations of hematite in South China Sea sediments

(Zhang *et al.* 2007), providing important information on regional climate change.

Here we apply this method to sediments from Hole U1456A. The sample preparation, analysis and data processing were performed at Nanjing University. All the dried samples were first ground in an agate mortar to a particle diameter of less than 30  $\mu\text{m}$ . We selected 19 samples for the calibration. For these calibration samples, iron oxides were removed by citrate–bicarbonate–dithionite (CBD) reagent (Mehra & Jackson, 1960) and the resulting residues provided a natural matrix material. Subsequently, known quantities of pigment-grade hematite were added to the matrix material to produce



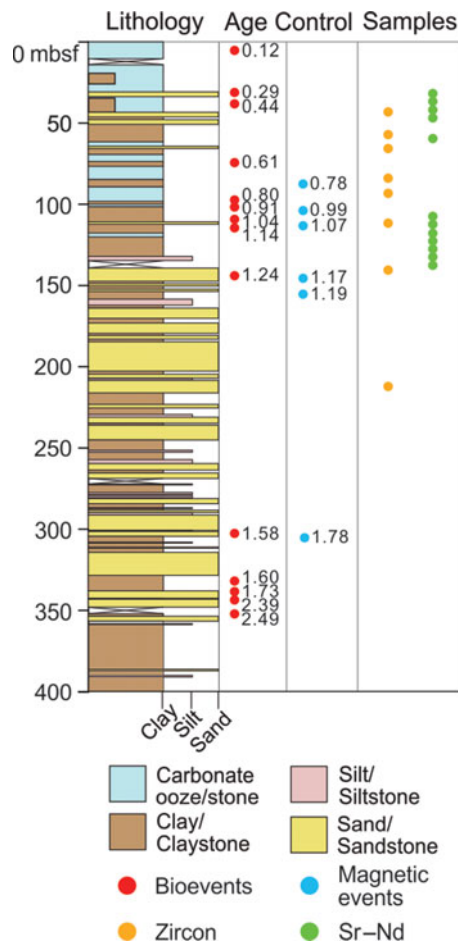


**Fig. 2.** (Colour online) Lithology and age controls of IODP Hole U1456A. Locations of samples for zircon and Sr–Nd analyses are represented by yellow and green dots, respectively (see Tables 1 and 2).

calibration standards. The hematite pigment used was standard Pfizer R1599 (Ji *et al.* 2002).

Reflectance spectra were analysed for 19 calibration samples and 908 actual samples from Site U1456A using a Perkin–Elmer Lambda 900 spectrophotometer (Perkin–Elmer Corporation, Norwalk, CT) with a diffuse reflectance attachment from 400 to 700 nm at 2 nm intervals. Reflectance data were processed to obtain percent reflectance in standard colour bands (Judd & Wyszecki, 1975), that is: violet, 400–450 nm; blue, 450–490 nm; green, 490–560 nm; yellow, 560–590 nm; orange, 590–630 nm; and red, 630–700 nm. Percent reflectance in the standard colour bands was calculated by dividing the percentage of reflectance in each colour band accordingly. Total reflectance of a sample or brightness was calculated by summing the reflectance value of a sample from 400 to 700 nm. For the calibration samples, a multiple linear regression model was built using the Statistical Product and Service Solutions (SPSS) program (<http://www.ndtimes.com.cn/news/162.html>) to relate independent variables (percent reflectance (%) in standard colour bands) to dependent variables (the known component values (wt%) of added hematite). The transfer function is defined: hematite (wt%) =  $4.203 - [0.271 \times \text{green} (\%)] + [0.167 \times \text{orange} (\%)]$  (coefficient of determination,  $R^2 = 0.886$ ). When we plot estimated hematite contents against

**Table 1.** Age control points from the biostratigraphy and palaeomagnetic stratigraphy data from Hole U1456A deposit sequence in east Arabian Sea (Pandey *et al.* 2016a, b)

	Depth (m)	Age (Ma)
<b>Fossils</b>		
<i>Globigerinoides ruber</i> pink	7.42	0.12
<i>Emiliania huxleyi</i>	28.60	0.29
<i>Pseudoemiliania lacunose</i>	37.56	0.44
<i>Globorotalia tosaensis</i>	75.04	0.61
Coiling change <i>Pulleniatina</i>	97.92	0.80
<i>Reticulofenestra asanoi</i>	99.24	0.91
reentrance <i>Gephyrocapsa</i> spp. > 4 $\mu\text{m}$	112.12	1.04
<i>Reticulofenestra asanoi</i>	119.19	1.14
<i>Gephyrocapsa</i> spp. > 5.5 $\mu\text{m}$	146.37	1.24
<i>Neogloboquadrina acostaeensis</i>	303.91	1.58
<i>Calcidiscus macintyreii</i>	329.365	1.60
<i>Gephyrocapsa</i> spp. > 5.5 $\mu\text{m}$	329.14	1.62
<i>Gephyrocapsa</i> spp. > 4 $\mu\text{m}$	330.67	1.73
<i>Discoaster brouweri</i>	342.90	1.93
<i>Discoaster pentaradiatus</i>	345.84	2.39
<i>Discoaster surculus</i>	353.06	2.49
<i>Sphaeroidinellopsis seminulina</i>	417.21	3.375
<b>Magnetostratigraphy</b>		
C1n(o)	87.01	0.781
C1r.1n(y)	105.03	0.988
C1r.1n(o)	117.02	1.072
C1r.2n(y)	152.84	1.173
C1r.2n(o)	158.22	1.185
C2n(y)	309.64	1.778

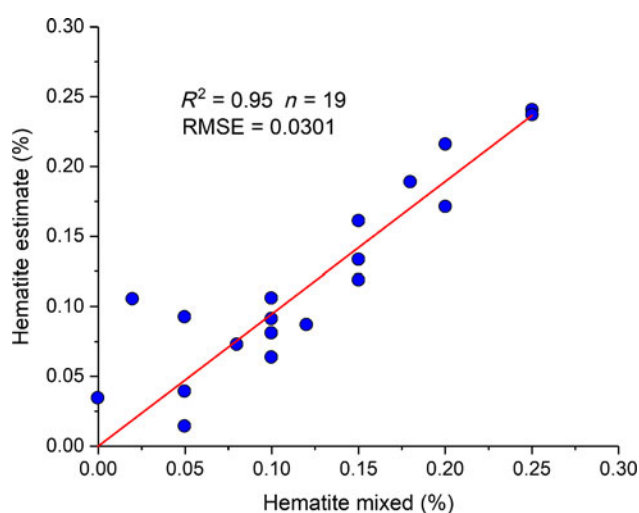
the actual iron oxide concentration mixed into the calibration samples (Fig. 3),  $R^2$  is 0.95 with a root mean square of error (RMSE) of 0.0301, where hematite concentration is within the range 0–0.25 wt%. The transfer function is therefore robust in providing reliable estimates of hematite in our sediments.

### 2.c. Zircon U–Pb dating and Sr–Nd isotopic composition analysis

Zircon U–Pb dating and Sr–Nd isotopic compositions are regarded as two of the best approaches for determining sediment provenance (Chen *et al.* 2007; Clift *et al.* 2008; Zhang *et al.* 2016, 2018). Because there are large differences in typical zircon U–Pb ages as well as in Sr–Nd isotopic compositions (DeCelles *et al.* 2000; Clift *et al.* 2002, 2019; Alizai *et al.* 2011) in tectonic blocks in South Asia, we can distinguish between the different sources in the eastern Arabian Sea deposits using these methods. We selected eight samples for zircon dating and 12 samples for Sr–Nd isotopic composition at Nanjing University. However, Sr isotopic composition is liable to change as a result of fractionation during chemical weathering (Derry & France-Lanord, 1996),

**Table 2.** Samples analysed for Sr–Nd isotopic composition and zircon particle dating

	Depth (m)	Age (Ma)
<b>Sr–Nd isotopic analysis</b>		
5H-5W-35/45	39.41	0.4186
6H-1W-25/35	42.76	0.4440
6H-2W-83/93	44.9	0.4602
7H-1W-140/150	53.45	0.5329
8H-5W-109/119	68.66	0.6408
13H-1W-85/85	109.86	0.9539
13H-3W-100/110	113.1	0.9796
14H-2W-80/90	120.86	1.0379
14H-5W-0/10	124.21	1.0629
15H-1W-65/75	128.76	1.0979
15H-5W-7/13	132.9	1.1290
17F-1W-20/30	139.56	1.1642
<b>Zircon dating</b>		
6H-5W	49	0.49
7H-5W	59	0.56
8H-2W	64	0.6
9H-5W	78	0.71
10H-5W	87	0.78
13H-3W	114	0.98
17F-1W	140	1.16
33F-1W	214	1.39

**Fig. 3.** (Colour online) Comparison between iron oxide content in the prepared samples with the predicted iron oxide content calculated according to the transfer function.

and shows some dependency on grain size (Meyer *et al.* 2011). Nd isotopes are stable during erosion and chemical weathering (Goldstein *et al.* 1984), but are known to be moderately

dependent on grain size variations in the Indus Basin (Jonell *et al.* 2018).

### 2.c.1. Zircon U–Pb dating

For each sample, standard water and magnetic separations were first used to extract heavy and non-magnetic minerals, from which more than 200 zircon grains were randomly picked using a microscope to ensure statistical adequacy (Andersen, 2005; Zhang *et al.* 2016, 2018). The zircon grains were then mounted in epoxy resin and polished for dating. All pre-treatments were performed by the same individual to make any artificial preference bias uniform.

The samples were measured using an Agilent 7700× inductively coupled plasma mass spectrometer (ICP-MS) with a New Wave 193-nm laser ablation system at Nanjing University. The laser beam diameter was 30 μm with a 10 Hz repetition rate (Zhang *et al.* 2018, 2016). Zircon 91500 was used as an external standard for isotopic fractionation correction, while NIST 610 (Pearce *et al.* 1997) was used as the standard for normalizing unknown U, Th and Pb content. Glitter 4.4.2 was used to process the raw ICP-MS data. Common Pb was corrected following the methods of Andersen (2002). We accept zircon ages that follow Andersen (2002), that is: (1) individual zircon discordance values are < 15%, which agrees with the concordant ages from published data of potential sources; and (2)  $^{206}\text{Pb}/^{238}\text{U}$  ages (or  $^{207}\text{Pb}/^{206}\text{Pb}$  ages for older grains) for zircon grains are < 1000 Ma. Most of the zircon samples measured in this study do not have the 110 minimum particles required by Vermeesch (2004), because at the fine grain size of these samples there were not enough particles large enough to date. We use the data as an approximate estimate of the sediment sources.

### 2.c.2. Sr–Nd isotopic composition analysis

The samples (c. 2 g) were first dissolved in 0.5 mol L<sup>-1</sup> acetic acids for 24 hours followed by 5% hydrogen peroxide for 24 hours to remove carbonates and organic matter, respectively. The remaining silicate fractions (c. 0.1 g) were digested in a mixture of HNO<sub>3</sub> and HF for 36 hours in tightly closed teflon vials at 115°C (Zhang *et al.* 2015). The digested solution was then loaded into ion-exchange columns to separate Sr and Nd elements using Sr-Spec, Ln-Spec and Tru-Spec resins (Aciego *et al.* 2009). The determination of Sr and Nd isotopes were performed by a Neptune plus multi-collector ICP-MS at Nanjing University.

The instrumental mass biases for Sr and Nd isotopes were corrected by normalizing the  $^{86}\text{Sr}/^{88}\text{Sr}$  ratio to 0.1194 and the  $^{146}\text{Nd}/^{144}\text{Nd}$  ratio to 0.7219, respectively. The Sr standard SRM987 and Nd standard JMCNd2O3 were periodically measured to check the reproducibility and accuracy of isotopic analyses with mean  $^{87}\text{Sr}/^{86}\text{Sr}$  ratio of  $0.710239 \pm 42$  ( $2\sigma$ ,  $n = 10$ ) and mean  $^{143}\text{Nd}/^{144}\text{Nd}$  ratio of  $0.512099 \pm 15$  ( $2\sigma$ ,  $n = 15$ ), respectively. The standard material BCR-2 was used to verify the chemical procedure. Measurements of 10 replicates yielded a mean  $^{87}\text{Sr}/^{86}\text{Sr}$  value of  $0.705018 \pm 20$  ( $2\sigma$ ,  $n = 10$ ) and a mean  $^{143}\text{Nd}/^{144}\text{Nd}$  value of  $0.512626 \pm 15$  ( $2\sigma$ ,  $n = 10$ ). Epsilon Nd ( $\epsilon_{\text{Nd}}$ ) values were calculated using chondritic values of  $^{143}\text{Nd}/^{144}\text{Nd} = 0.512638$ .

## 3. Results

The results of zircon U–Pb ages (Fig. 4), DRS, hematite content estimation and grain size (Figs 5–7), as well as Sr–Nd isotopic composition (Table 3, Fig. 8), are presented. The distributions of zircon U–Pb ages for all the samples are similar through time, with most ages distributed between 0–200 Ma and 300–1000 Ma (Fig. 4).

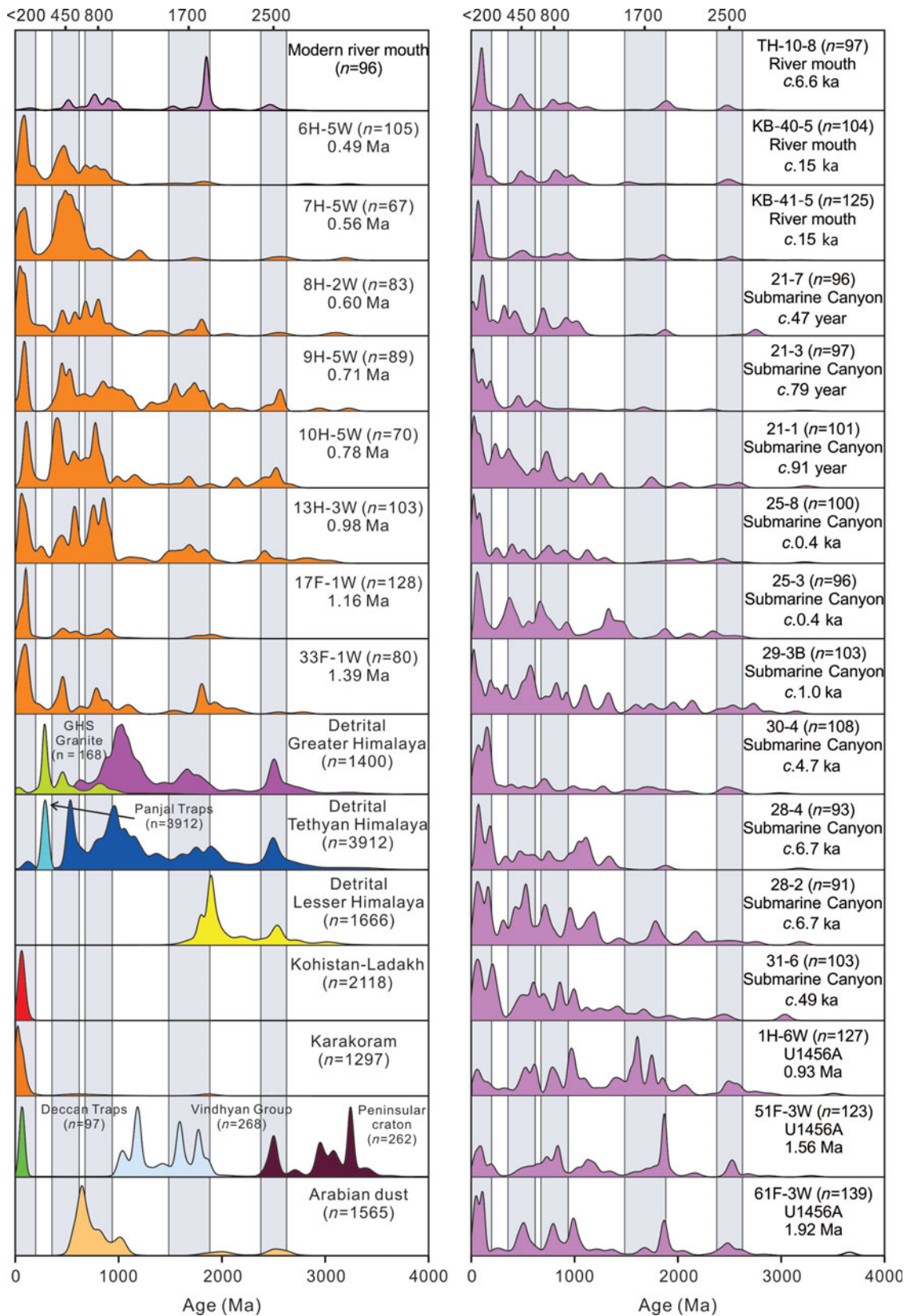


**Fig. 4.** (Colour online) Kernel density estimates for U-Pb zircon age distributions of samples from U1456A (orange) in this study and potential sources (see online Supplementary Table S1, available at <http://journals.cambridge.org/geo>), compared with samples from previous studies (violet) including Indus River mouth (Clift *et al.* 2008), IODP 355 (Clift *et al.* 2019) and Indus Submarine Canyon (Li *et al.* 2018). Peak ages are shown at the top (Ma).

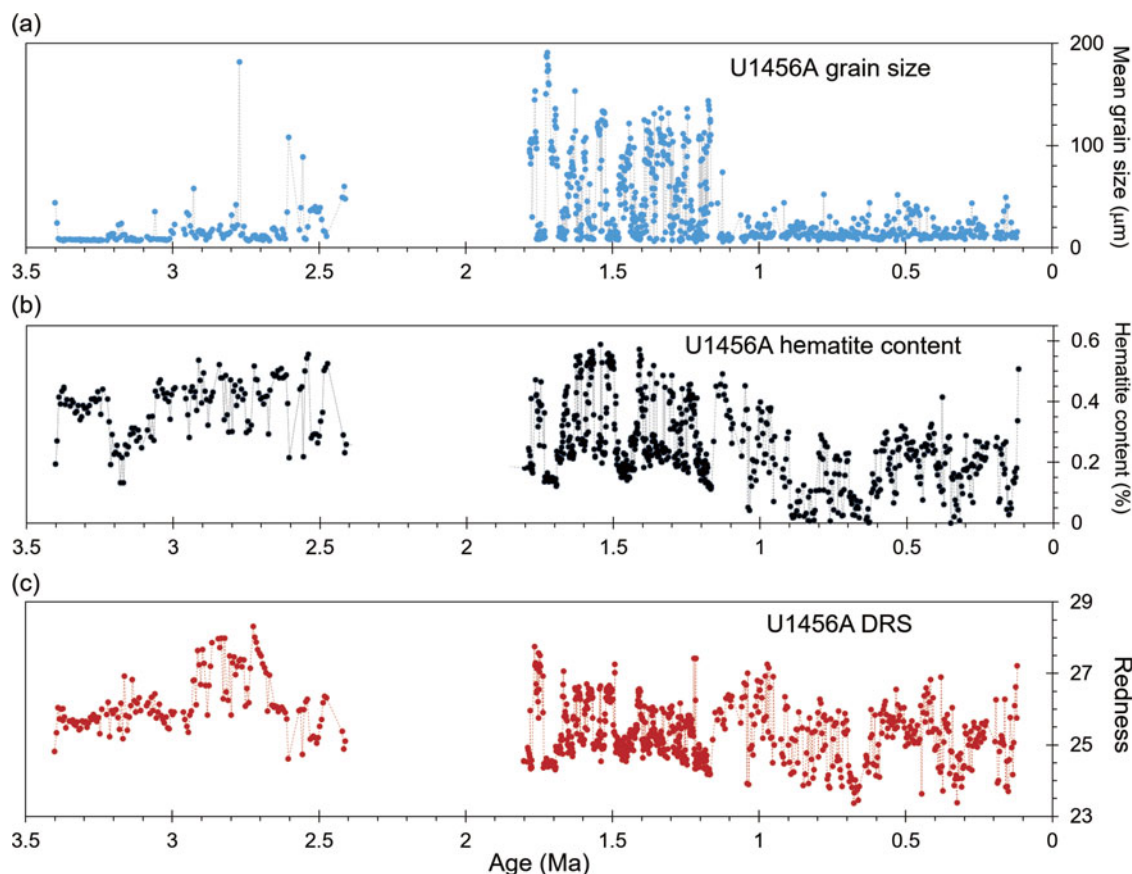


Fig. 5. (Colour online) (a) Grain size, (b) hematite content and (c) DRS variations from Hole U1456A deposit sequence since late Pliocene time (c. 3.4 Ma).

$\epsilon_{\text{Nd}}$  values range between  $-12.8$  and  $-8.7$  and  $^{86}\text{Sr}/^{87}\text{Sr}$  varies between  $0.727230$  and  $0.713162$  (Table 3, Fig. 8). Grain size is highly variable over the range  $5.9$ – $190.8$   $\mu\text{m}$ , with an average mean value of  $36.0$   $\mu\text{m}$  (Fig. 5) (Liu *et al.* 2018). The hematite content varied over  $0.00$ – $0.59\%$  with an average of  $0.27\%$  (Fig. 5), and was coupled with grain size over glacial–interglacial cycles and the longer timescale, in particular during c.  $1.8$ – $1.1$  Ma (Fig. 6). Both hematite content and grain size show a three-step evolution, comprising phases of  $3.4$ – $2.4$  Ma,  $1.8$ – $1.1$  Ma and  $1.1$ – $0.1$  Ma (Figs 5–7).

## 4. Discussion

### 4.a. Provenance of deposits and implication for erosion

The identification of NW–SE-aligned deep-sea channel systems in Laxmi Basin supports the idea that most deposits in the basin were supplied from the Indus drainage basin (Fig. 1c) (Mishra *et al.* 2016; Pandey *et al.* 2016a; Clift *et al.* 2019; Yu *et al.* 2019). Five main tectonic blocks – Greater Himalaya, Tethyan Himalaya, Lesser Himalaya, Karakoram and Karakoram–Kohistan–Ladakh (KKL) (Fig. 1b) – characterize sediment composition in the Indus River drainage basin. Each block has a different provenance proxy character. The zircon age distribution and Sr–Nd isotopic composition of these blocks are presented in Figures 4, 8 and 9. The Himalayan blocks (including the Greater Himalaya, Tethyan

Himalaya and Lesser Himalaya) have much more radiogenic  $\epsilon_{\text{Nd}}$  and  $^{87}\text{Sr}/^{86}\text{Sr}$  values, and older zircon ages (mainly  $> 300$  Ma, with  $520$ – $600$ ,  $800$ – $1000$ ,  $1600$ – $1800$  and c.  $2500$  Ma peaks for Himalaya sedimentary and metamorphic rocks and c.  $290$ , c.  $450$  and c.  $800$  Ma for Himalayan granites; Fig. 4). In contrast, the KKL, which is located within the Eurasian Plate, has less radiogenic  $\epsilon_{\text{Nd}}$  and  $^{87}\text{Sr}/^{86}\text{Sr}$  values and younger zircon ages, mostly  $< 200$  Ma (Figs 4, 8). The zircon age distribution of Hole U1456A sediments is characterized by peaks of  $< 200$ , c.  $450$ , c.  $800$ ,  $1600$ – $1800$  and c.  $2500$ , suggesting mixed sediment sources from at least two end-members from both the KKL and the Greater, Tethyan and Lesser Himalaya (Figs 4, 9). The  $\epsilon_{\text{Nd}}$  and  $^{87}\text{Sr}/^{86}\text{Sr}$  values of sediments at Hole U1456A fall roughly in the middle between the bedrocks of the Himalaya (mainly the Greater and Tethyan Himalaya) and the KKL (Fig. 8), in agreement with our interpretations for the zircon data (Figs 4, 9).

The other potential sediment sources for deposits in Laxmi Basin were the Indian Peninsula (including the Deccan Traps, Vindhyan Group and the Peninsular Craton; Fig. 1a) and eolian dust from the Arabian Peninsula. However, we argue that these sources were not the major contributions to sediments in Laxmi Basin for the following reasons.

First, some of the zircon age peaks (c.  $1150$  Ma in the Vindhyan Group and  $> 3000$  Ma in the Peninsular Craton; Fig. 4) of the tectonic blocks in the Indian Peninsula are not prominent



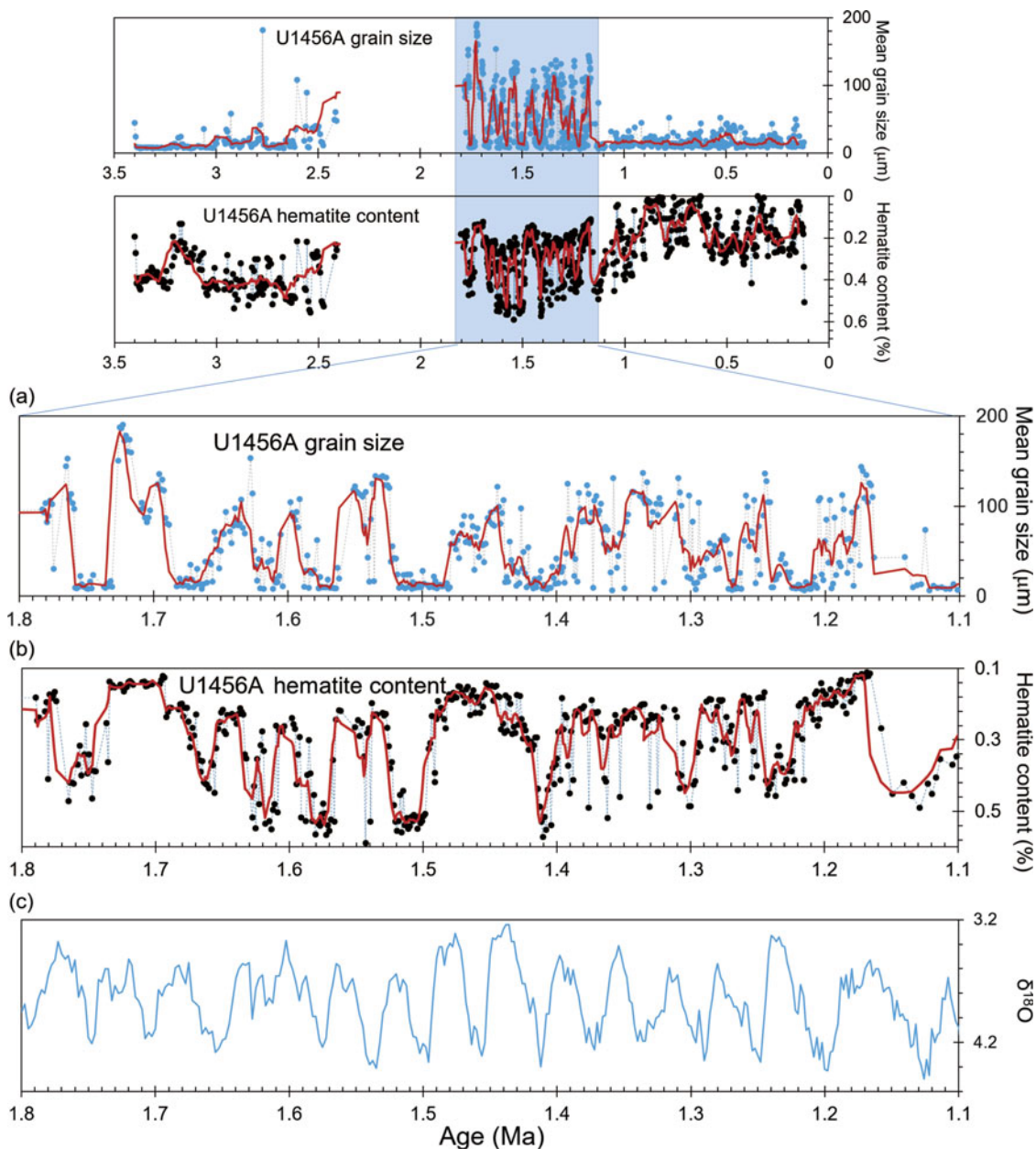


**Fig. 6.** (a) Grain size and (b) hematite content for Hole U1456A deposit sequence, and (c) global ice volume and temperature (Lisiecki & Raymo, 2005) during 1.8–1.1 Ma.

in sediments at Hole U1456A, precluding their major contribution to the Laxmi Basin. The Deccan Traps are characterized by *c.* 65 Ma zircon ages (Fig. 4) and have much lower radiogenic  $\epsilon_{\text{Nd}}$  and  $^{87}\text{Sr}/^{86}\text{Sr}$  values than Hole U1456A sediments (Fig. 8). The Deccan Traps are not a major provenance candidate for the sands at Hole U1456A, but could have supplied some of the finer-grained material (Clift *et al.* 2019; Yu *et al.* 2019). Arabian dust has similar zircon age distributions to Hole U1456A deposits (Fig. 4), but is characterized by a wide range of  $^{87}\text{Sr}/^{86}\text{Sr}$  values and less radiogenic  $\epsilon_{\text{Nd}}$  values, meaning it is dissimilar to the U1456A deposits (Figs 8, 9).

Second, no active deep-sea channel system has yet been identified along the western margin of the Indian Peninsula (Fig. 1c, d; Mishra *et al.* 2016), suggesting that the rivers from the Indian Peninsula do not transport large volumes of coarse-grained

sediments as far as the Laxmi Basin. This is probably because the extremely broad shelf on the western continental margin of the Indian Peninsula buffers river-transported sediments (Fig. 1a), although deposition of fine-grained sediment from hypopycnal plumes is still possible.

Third, the Tapti and Narmada rivers draining the Indian Peninsula contribute more sediments to the Arabian Sea than the Indus River at present (Khim *et al.* 2019), but the reduction of the Indus River contribution could be caused by human activity such as building dams along the Indus River (Mahar & Zaigham, 2014). The damming is quite recent and had no impact on the sediment input to the Arabian Sea in the geological past.

The abovementioned points suggest that the sediments at Hole U1456A were mainly derived by erosion from the Himalaya–Karakoram Mountains via the Indus River. There were contributions



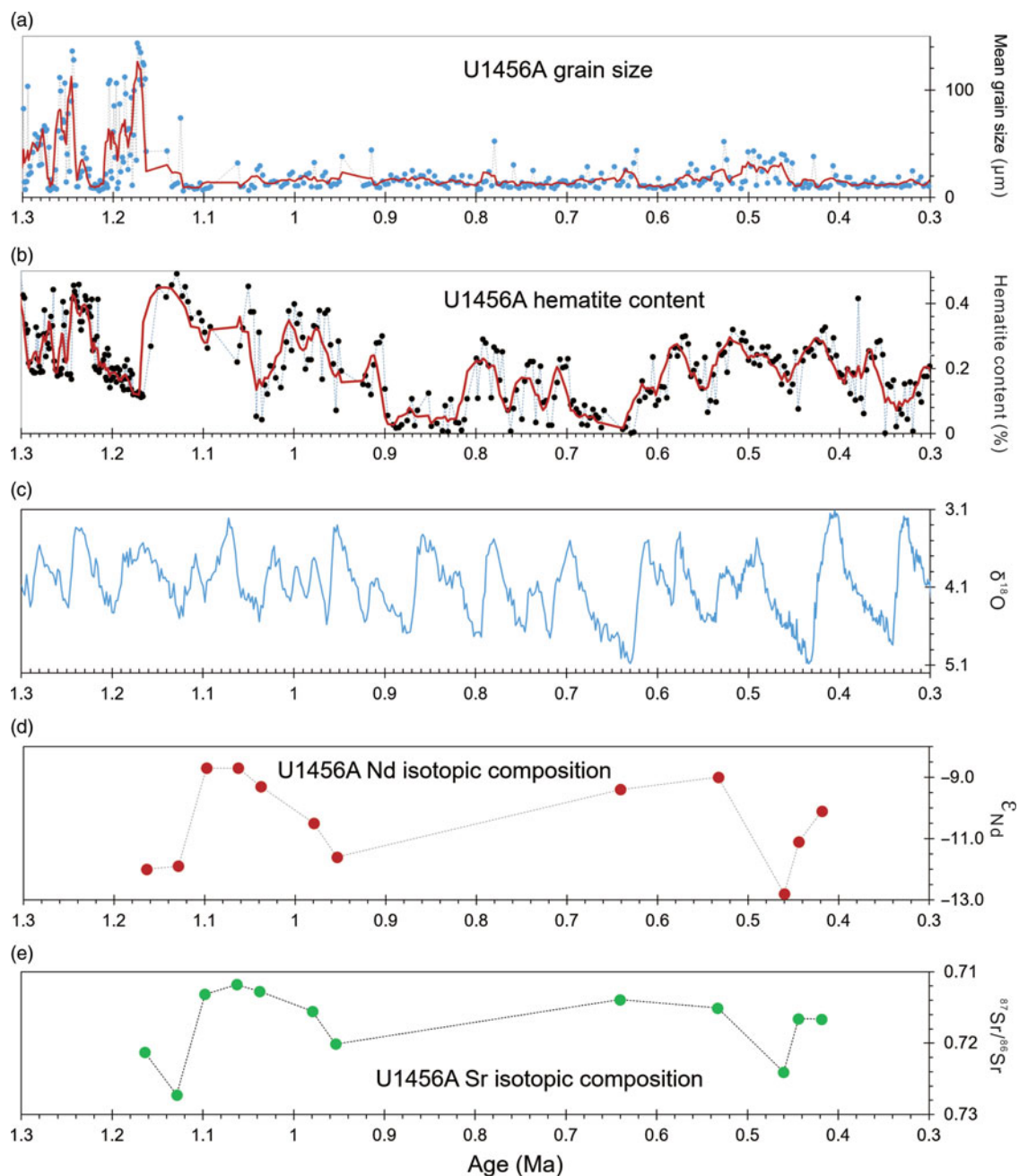


**Fig. 7.** (a) Grain size, (b) hematite content, (c) global ice volume and temperature (Lisiecki & Raymo, 2005), (d) Nd and (e) Sr isotopic composition variations for Hole U1456A deposition sequence during 1.1–0.3 Ma.

from the Arabian Peninsula and the Indian Peninsula, but these were not the dominant sources (Figs 4, 8).

#### 4.b. Changes of sediment provenance during glacial–interglacial cycles

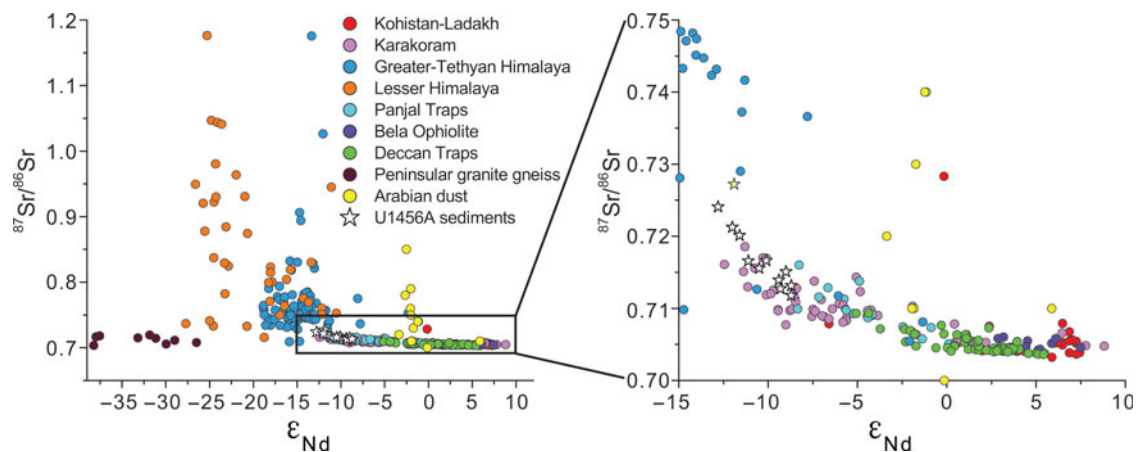
The surface sediments eroded from the Himalaya–Karakoram Mountains could not be instantaneously deposited in the deep Arabian Sea because of the long-distance transport from source to sink, during which sediment recycling and mixing would occur. It is possible that most of the sediments were stored on the continental shelf for a long time and that the fan deposits

must therefore have lagged the erosion processes onshore (Covault *et al.* 2013). In the Holocene Indus canyon, the lag time for fine-grained Holocene sediment between the canyon and the river mouth was < 10 ka (Li *et al.* 2018). Holocene sediments in Indus Canyon isotopically resemble deposits in the Indus River mouth since *c.* 8 ka. However, fine sediment only reached the canyon and not the upper fan during the Holocene period, and would be expected to be redeposited when sea level fell during the following glaciations, possibly after *c.* 100 ka. In addition, sand in the canyon is not similar to that from the river mouth in terms of zircon U–Pb ages, suggesting that sand is stored near the river mouth and is only reworked into the fan

**Table 3.** Sr–Nd isotopic compositions of samples from Hole U1456A

Sample no.	Sample label	Age (Ma)	$^{143}\text{Nd}/^{144}\text{Nd}$	$\pm 2\sigma$	$\epsilon_{\text{Nd}}^a$	$^{87}\text{Sr}/^{86}\text{Sr}$	$\pm 2\sigma$
1	5H-5W-35/45	0.4186	0.512120	3	−10.1	0.716648	7
2	6H-1W-25/35	0.4440	0.512068	3	−11.1	0.716569	6
3	6H-2W-83/93	0.4602	0.511984	4	−12.8	0.724076	7
4	7H-1W-140/150	0.5329	0.512175	7	−9.0	0.715093	7
5	8H-5W-109/119	0.6408	0.512158	5	−9.4	0.713926	8
6	13H-1W-85/85	0.9539	0.512046	4	−11.6	0.720125	8
7	13H-3W-100/110	0.9796	0.512102	6	−10.5	0.715555	6
8	14H-2W-80/90	1.0379	0.512163	8	−9.3	0.712736	8
9	14H-5W-0/10	1.0629	0.512192	8	−8.7	0.711788	7
10	15H-1W-65/75	1.0979	0.512194	9	−8.7	0.713162	7
11	15H-5W-7/13	1.1290	0.512028	8	−11.9	0.727230	7
12	17F-1W-20/30	1.1642	0.512023	7	−12.0	0.721257	9

<sup>a</sup>  $\epsilon_{\text{Nd}}$  values calculated using chondritic values of  $^{143}\text{Nd}/^{144}\text{Nd} = 0.512638$ ;  $\epsilon_{\text{Nd}} = [(^{143}\text{Nd}/^{144}\text{Nd} - 0.512638) / 0.512638] \times 10000$ .

**Fig. 8.** (Colour online) Sr–Nd isotopic composition of selected samples from Hole U1456A (white stars) and potential sediment sources in SW Asia.

during sea-level lowstands, potentially on timescales of 100 ka (Li *et al.* 2019).

The other recycling scenario is one in which turbidite flow was episodic and transport of sediments was accompanied by mixing older and younger deposits. However, the turbidite events in the Indus deep-sea fan are estimated to have occurred every *c.* 5–10 ka during the past 100 ka (Bourget *et al.* 2013). The turbidite events in the sub-basin analysed by Bourget *et al.* (2013) occurred much less frequently than those of glacial–interglacial alternations (100–400 ka), although coring suggests that much of the upper fan has been inactive since 11 ka (Prins *et al.* 2000). More frequent turbidites on the lower fan, such as those dated by Bourget *et al.* (2013), cannot be sourced from the Indus Canyon or River. Sediment recycling and mixing processes could have resulted in mixed sediment spanning glacial or interglacial phases.

Our results show small source shifts at the glacial–interglacial alternations, demonstrated by the Nd–Sr isotopic composition (Table 3, Fig. 7). The range of compositions lies within those noted

by Yu *et al.* (2019), and closer to the interglacial end-member composition of the Indus River noted by Li *et al.* (2018). Given that no major tectonic deformation occurred over such short periods, and no drainage system reorganization occurred (Clift, 2017), the variations may not be interpreted by tectonic forcing. A possible reason for the changing sediment sources may be the migration of the maximum monsoon rainfall belt, associated with global temperature and the glacial–interglacial cycles, and documented to have forced a shift in sediment source since the Last Glacial Maximum (Clift *et al.* 2008). The samples with the most negative  $\epsilon_{\text{Nd}}$  values are interpreted to be dominated by erosion from the Himalayan ranges. This probably occurred during interglacial periods when the monsoon rainfall is focused in the Lesser Himalaya, so that relatively less sediment is derived from the KKL region (Fig. 1a). During glacial times it seems erosion is more dominated by the Karakoram;  $\epsilon_{\text{Nd}}$  values are higher in this case, which may be caused by the monsoon rainfall belt and the migrations of westerlies (Clift *et al.* 2019), but further investigation is required.

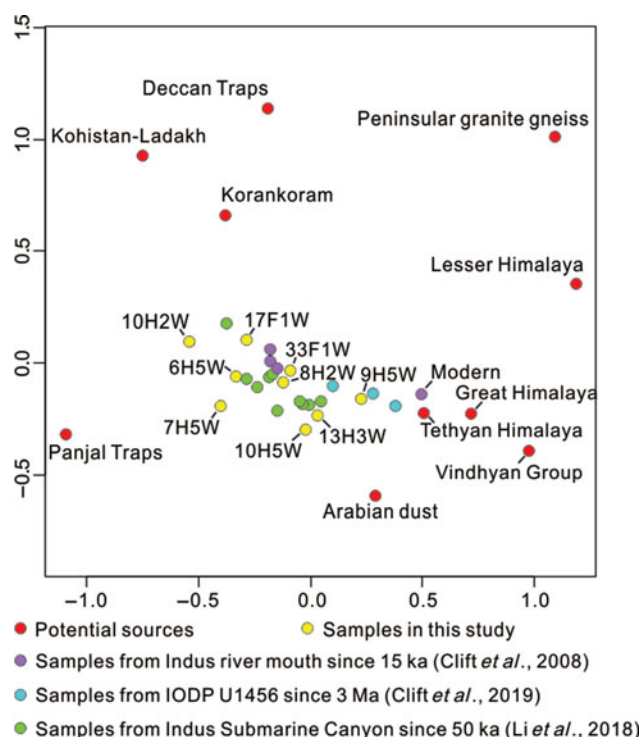


**Fig. 9.** (Colour online) Multidimensional scaling map based on calculated Kolmogorov–Smirnov test between U–Pb age spectra, showing samples of U1456A in this study compared with samples from previous studies, including Indus River mouth (Clift *et al.* 2008), IODP Expedition 355 (Clift *et al.* 2019) and Indus Submarine Canyon (Li *et al.* 2018). Samples and sources with similar U–Pb age distributions are plotted closer together.

#### 4.c. SASM precipitation variations at tectonic timescales from late Pliocene time

The SASM variation at glacial–interglacial timescales has been well documented (Prell & Kutzbach, 1987; Clemens & Oglesby, 1992; Gupta *et al.* 2005; Clemens *et al.* 2010). Insolation, global ice volume (global temperature), sea level and Southern Hemisphere atmospheric circulation have been hypothesized to force monsoon variations. However, the debate concerning monsoon variations in terms of both timing and intensity continues. At longer timescales (longer than orbital timescales), the relationship between climate, erosion and tectonics is not clear because of a lack of high-resolution records of these processes. Here, we use hematite content and grain size as indicators of regional aridity and deep-sea depositional environment (Figs 5–7) that were associated with the SASM at the orbital timescale. Hematite ( $\alpha\text{-Fe}_2\text{O}_3$ ) favours a dry and warm climate (Ji, 2004). Moreover, sediment particles transported from the Indus River might be expected to be coarser grained during times of greater runoff, although this is stored near the river mouth and does not reach the deep sea during the interglacial highstands (Li *et al.* 2019). However, sediment budgets for the last deglacial period indicate that the vast majority of sediments reaching the ocean were stored in delta and shelf clinoforms (Clift & Giosan, 2014). This implies that the large-scale redeposition into deeper water occurred during sea-level lowstands when the climate was cold (Prins *et al.* 2000). The Holocene carbonate drape found over much of the upper fan (Kolla *et al.* 1981) was consistent with this and indicated that sedimentation on the deep-sea fan, including the

Laxmi Basin, is at least partly controlled by sea level. It is well established that global temperature, sea level and monsoon precipitation vary synchronously with glacial–interglacial cycles in South Asia (Wang *et al.* 2017), and that sea level and monsoon precipitation also co-vary with glacial–interglacial alternation. In this case, the hematite content and grain size indicated variations in sea level and depositional environment, and therefore changes in the SASM.

It is apparent that the SASM experienced three distinct phases since late Pliocene time (*c.* 3.4 Ma), associated with the glacial–interglacial alternations based on our grain size and hematite records (Figs 5–7). A phase with low monsoon precipitation and medium variation in monsoon amplitude occurred during *c.* 3.4–2.4 Ma, followed by increased precipitation and amplitude variation at 1.8–1.1 Ma, and finally reduced precipitation and amplitude variation during 1.1–0.1 Ma. Hematite content has also undergone three phases (Fig. 5): sediment high in hematite was deposited during 3.4–2.4 Ma, intermediate in hematite during *c.* 1.8–1.1 Ma and low in hematite during 1.1–0.1 Ma.

#### 4.d. Variations in SASM precipitation, weathering and surface erosion

We undertook spectral and cross-spectral analyses of the hematite content and grain-size time series (Fig. 10). The cycles of periods *c.* 100 and *c.* 41 ka, dominated by sea level and insolation, were evident and exceeded 90% confidence levels, showing that the weathering intensity and stream flow transporting the sediments varied with these orbital frequencies. In the frequency domain, anti-phase variations of the grain size and hematite content provide some clues concerning the forcing mechanism for changes in sea level, the SASM and surface erosion. We suggest that the co-variations in hematite content and grain-size changes may have been controlled by sea-level changes since late Pliocene time, and that sea-level changes were closely associated with the SASM intensity at tectonic and orbital timescales; these proxy indicators therefore describe the long-term evolution of the SASM (Figs 5–7).

Our multi-technique analyses of sediment proxies from Hole U1456A show varying sea level, SASM precipitation and weathering intensity in SW Asia over orbital-dominated cycles (Fig. 10). The co-variations between the weathering intensity and sea level provide direct evidence that sea level and associated monsoon circulation controlled the environmental variation over glacial–interglacial alternations.

## 5. Conclusions

On the basis of our new data, the evolution of the SASM precipitation and weathering intensity in the Himalaya–Karakoram Mountains can be divided into three phases since late Pliocene time. Weak summer monsoon precipitation with small amplitude fluctuations and enhanced formation of hematite occurred during *c.* 3.4–2.4 Ma; increased monsoon rainfall, with greater variation in amplitude as shown by variability in hematite content, occurred during 1.8–1.1 Ma; and average monsoon rainfall decreased and experienced small variations in amplitude, as tracked by hematite formation, during 1.1–0.1 Ma. We interpret our results to indicate that sea level and weathering intensity co-varied with the glacial–interglacial alternations since late Pliocene time, in particular at 1.8–1.1 Ma, in SW Asia. Variations of hematite content and grain size were originally determined by weathering intensity, monsoon



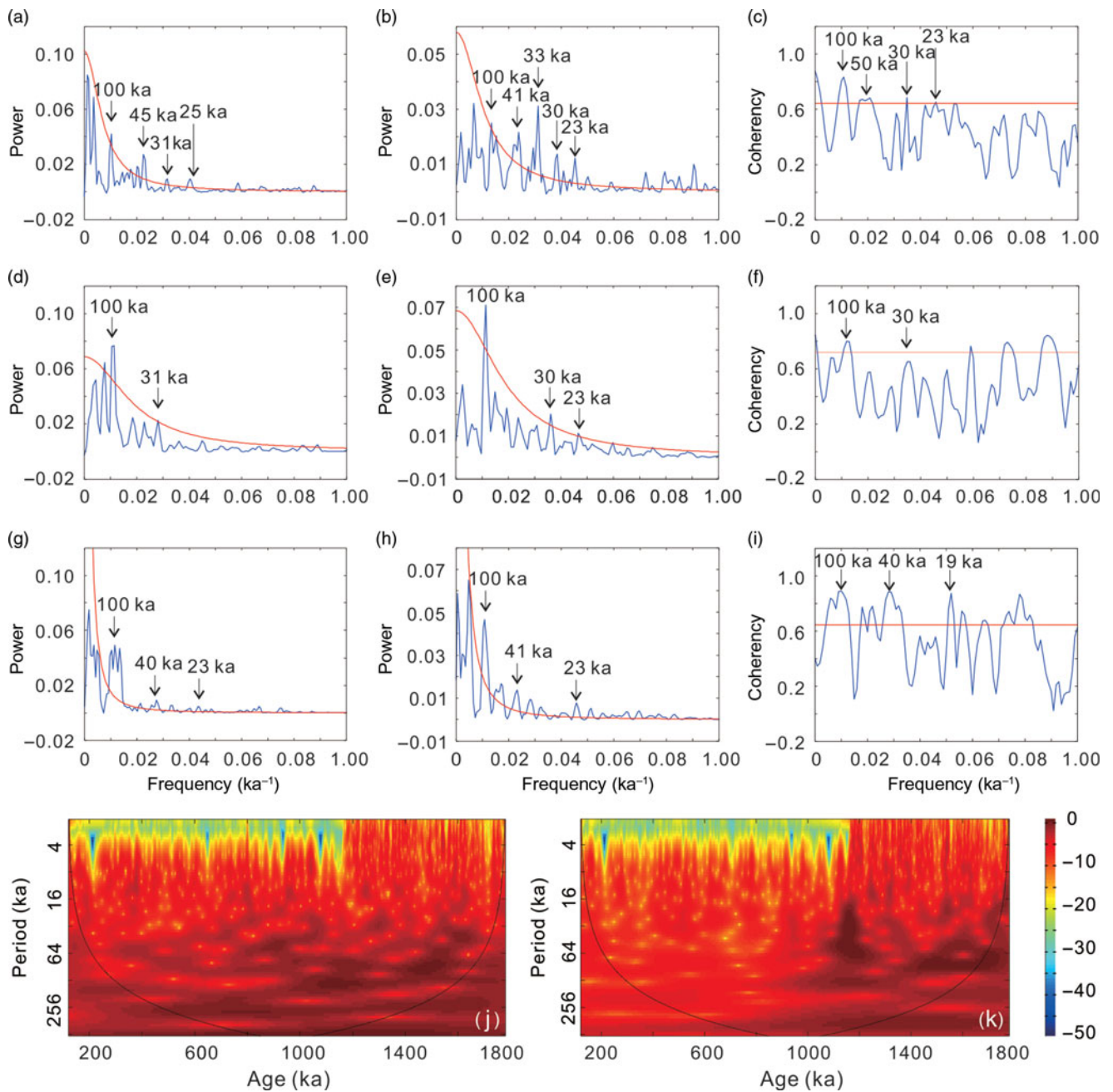


**Fig. 10.** (Colour online) Spectral analysis, cross-spectral analysis and wavelet transforms of the hematite content and grain-size time series since c. 3.4 Ma (blue curves) with red lines showing the 90% confidence level. Spectral analyses of (a, g, e) hematite content and (b, e, h) grain size time series, and (c, f, i) cross-spectral analysis between these two records during (a–c) 1.1–0.1 Ma, (d–f) 1.8–1.1 Ma and (g–i) 3.4–2.4 Ma. The lower panels represent the evolving spectrum power with time derived from wavelet transform of (left) hematite content and (right) grain size time series during 1.8–0.1 Ma.

rainfall and runoff velocity, and were modulated by changes in sea level and ocean environment. Our findings demonstrate the interplay between monsoon precipitation, mountain weathering and surface erosion over tectonic and glacial–interglacial timescales in SW Asia.

**Acknowledgements.** We thank China-IODP for supporting HY Lu to participate in the IODP 355 expedition during April–June 2015 in the Arabian Sea. This research is supported by the National Natural Science Foundation of China (grant nos 41888101, 41690111 and 41920104005) and the post-cruise research grant to HY Lu.

**Supplementary material.** To view supplementary material for this article, please visit <https://doi.org/10.1017/S0016756820000291>

## References

- Aciego SM, Bourdon B, Lupker M and Rickli J (2009) A new procedure for separating and measuring radiogenic isotopes (U, Th, Pa, Ra, Sr, Nd, Hf) in ice cores. *Chemical Geology* **266**, 194–204.
- Alizai A, Carter A, Clift PD, Vanlaningham S, Williams JC and Kumar R (2011) Sediment provenance, reworking and transport processes in the

- Indus River by U–Pb dating of detrital zircon grains. *Global and Planetary Change* **76**, 33–55.
- Amir A, Kenyon NH, Cramp A and Kidd RB** (1996) Morphology of channel-levée system on the Indus deep-sea fan, Arabian Sea. *Pakistan Journal of Hydrocarbon Research* **8**, 43–53.
- Andersen T** (2002) Correction of common lead in U–Pb analyses that do not report <sup>204</sup>Pb. *Chemical Geology* **192**, 59–79.
- Andersen T** (2005) Detrital zircons as tracers of sedimentary provenance: limiting conditions from statistics and numerical simulation. *Chemical Geology* **216**, 249–70.
- Balsam WL and Deaton BC** (1996) Determining the composition of late Quaternary marine sediments from NUV, VIS, and NIR diffuse reflectance spectra. *Marine Geology* **134**, 31–55.
- Betzler C, Eberli GP, Kroon D, Wright JD, Swart PK, Nath BN, Alvarez-Zarikian CA, Alonso-García M, Bialik OM, Blättler CL, Guo JA, Haffen S, Horozal S, Inoue M, Jovane L, Lanci L, Laya JC, Mee ALH, Lüdmann T, Nakakuni M, Niino K, Petruny LM, Pratiwi SD, Reijmer JJG, Reolid J, Slagle AL, Sloss CR, Su X, Yao Z and Young JR** (2016) The abrupt onset of the modern South Asian Monsoon winds. *Scientific Reports* **7**, 29838.
- Blöthe JH, Munack H, Korup O, Fülling A, Garzanti E, Resentini A and Kubik PW** (2014) Late Quaternary valley infill and dissection in the Indus River, western Tibetan Plateau margin. *Quaternary Science Reviews* **94**, 102–19.
- Boos WR and Kuang Z** (2010) Dominant control of the South Asian monsoon by orographic insulation versus plateau heating. *Nature* **463**, 218–22.
- Botsyun S, Sepulchre P, Donnadiou Y, Risi C, Licht A and Rugenstein JKC** (2019) Revised paleoaltimetry data show low Tibetan Plateau elevation during the Eocene. *Science*, **363**, eaaq1436, doi: [10.1126/science.aaq1436](https://doi.org/10.1126/science.aaq1436).
- Bourget J, Zaragosi S, Rodriguez M, Fournier M, Garlan T and Chamot-Rooke N** (2013) Late Quaternary megaturbidites of the Indus fan: origin and stratigraphic significance. *Marine Geology* **336**, 10–23.
- Chen J, Li G, Yang J, Rao W, Lu H, Balsam W, Sun Y and Ji J** (2007) Nd and Sr isotopic characteristics of Chinese deserts: implications for the provenances of Asian dust. *Geochimica et Cosmochimica Acta* **71**, 3904–14.
- Clemens SC and Oglesby RJ** (1992) Interhemispheric moisture transport in the Indian Ocean summer monsoon: data-model and model-model comparisons. *Paleoceanography* **7**, 633–43.
- Clemens SC, Prell WL and Sun Y** (2010) Orbital-scale timing and mechanisms driving Late Pleistocene Indo-Asian summer monsoons: reinterpreting cave speleothem  $\delta^{18}\text{O}$ . *Paleoceanography* **25**, PA4207.
- Clift PD** (2017) Cenozoic sedimentary records of climate-tectonic coupling in the Western Himalaya. *Progress in Earth and Planetary Science* **4**(39), 1–22.
- Clift PD and Giosan L** (2014) Sediment fluxes and buffering in the post-glacial Indus Basin. *Basin Research* **26**, 369–86.
- Clift PD, Giosan L, Blusztajn J, Campbell IH, Allen C, Pringle M, Tabrez AR, Danish M, Rabbani MM and Alizai A** (2008) Holocene erosion of the Lesser Himalaya triggered by intensified summer monsoon. *Geology* **36**, 79–82.
- Clift PD, Lee JJ, Hildebrand P, Shimizu N, Layne GD, Blusztajn J, Blum JD, Garzanti E and Khan AA** (2002) Nd and Pb isotope variability in the Indus River System: implications for sediment provenance and crustal heterogeneity in the Western Himalaya. *Earth and Planetary Science Letters* **200**, 91–106.
- Clift PD and Vanlaningham S** (2010) A climatic trigger for a major Oligo-Miocene unconformity in the Himalayan foreland basin. *Tectonics* **29**, TC5014.
- Clift PD, Wan S and Blusztajn J** (2014) Reconstructing chemical weathering, physical erosion and monsoon intensity since 25Ma in the northern South China Sea: a review of competing proxies. *Earth-Science Reviews* **130**, 86–102.
- Clift PD, Zhou P, Stockli DF and Blusztajn J** (2019) Regional Pliocene exhumation of the Lesser Himalaya in the Indus drainage. *Solid Earth* **10**, 647–61, doi: [10.5194/se-10-647-2019](https://doi.org/10.5194/se-10-647-2019).
- Colin C, Turpin L, Bertaux J, Desprairies A and Kissel C** (1999) Erosional history of the Himalayan and Burman ranges during the last two glacial-interglacial cycles. *Earth and Planetary Science Letters* **171**, 647–60.
- Covault JA, Craddock WH, Romans BW, Fildani A and Gosai M** (2013) Spatial and temporal variations in landscape evolution: historic and longer-term sediment flux through global catchments. *Journal of Geology* **121**, 35–56.
- Deaton BC and Balsam WL** (1991) Visible spectroscopy; a rapid method for determining hematite and goethite concentration in geological materials. *Journal of Sedimentary Research* **61**, 628–32.
- DeCelles PG, Gehrels GE, Quade J, Lareau B and Spurlin M** (2000) Tectonic implications of U–Pb zircon ages of the Himalayan orogenic belt in Nepal. *Science* **288**, 497–9.
- Derry LA and France-Lanord C** (1996) Neogene Himalayan weathering history and river <sup>87</sup>Sr/<sup>86</sup>Sr; impact on the marine Sr record. *Earth and Planetary Science Letters* **142**, 59–74.
- Goldstein SL, O’Nions RK and Hamilton PJ** (1984) A Sm–Nd isotopic study of atmospheric dusts and particulates from major river systems. *Earth and Planetary Science Letters* **70**, 221–36.
- Goodbred SL and Kuehl SA** (2000) Enormous Ganges-Brahmaputra sediment discharge during strengthened early Holocene monsoon. *Geology* **28**, 1083–6.
- Gupta AK, Das M and Anderson DM** (2005) Solar influence on the Indian summer monsoon during the Holocene. *Geophysical Research Letters* **32**, L17703.
- Gupta AK, Yuvaraja A, Prakasam M, Clemens SC and Velu A** (2015) Evolution of the South Asian monsoon wind system since the late Middle Miocene. *Palaeogeography, Palaeoclimatology, Palaeoecology* **438**, 160–7.
- Huber M and Goldner A** (2012) Eocene monsoons. *Journal of Asian Earth Sciences* **44**, 3–23, doi: [10.1016/j.jseas.2011.09.014](https://doi.org/10.1016/j.jseas.2011.09.014).
- Ji J** (2004) High resolution hematite/goethite records from Chinese loess sequences for the last glacial-interglacial cycle: rapid climatic response of the East Asian Monsoon to the tropical Pacific. *Geophysical Research Letters* **31**, 171–4.
- Ji J, Balsam W, Chen JU and Liu L** (2002) Rapid and quantitative measurement of hematite and goethite in the Chinese loess-paleosol sequence by diffuse reflectance spectroscopy. *Clays and Clay Minerals* **50**, 208–16.
- Jonell TN, Carter A, Böning P, Pahnke K and Clift PD** (2017) Climatic and glacial impact on erosion patterns and sediment provenance in the Himalayan rain shadow, Zaskar River, NW India. *Geological Society of America Bulletin* **129**, 820–36.
- Jonell TN, Li Y, Blusztajn J, Giosan L and Clift PD** (2018) Signal or noise? Isolating grain size effects on Nd and Sr isotope variability in Indus delta sediment provenance. *Chemical Geology* **485**, 56–73.
- Judd DB and Wyszecski G** (1975) *Color in Business, Science, and Industry*. New York: John Wiley & Sons, 553 pp.
- Kenyon NH, Amir A and Cramp A** (1995) Geometry of the younger sediment bodies of the Indus Fan. In *Atlas of Deep Water Environments: Architectural Style in Turbidite System* (eds KT Pickering, RN Hiscott, NH Kenyon, F Ricci Lucchi and RDA Smith), pp. 89–93. London: Chapman & Hall.
- Khim B-K, Horikawa K, Asahara Y, Kim J-E and Ikehara M** (2019) Detrital Sr–Nd isotopes, sediment provenances, and depositional processes in the Laxmi Basin of the Arabian Sea during the last 800 ka. *Geological Magazine*, published online 23 November 2018, doi: [10.1017/S0016756818000596](https://doi.org/10.1017/S0016756818000596).
- Kodagali VN and Jauhari P** (1999) The meandering Indus channels: study in a small area by the multibeam swath bathymetry system – Hydrosweep. *Current Science* **76**(2), 240–43.
- Kolla V, Ray PK and Kostecki JA** (1981) Surficial sediments of the Arabian Sea. *Marine Geology* **41**, 183–204.
- Kroon D, Steens T and Troelstra SR** (1991) Onset of monsoonal related upwelling in the western Arabian Sea as revealed by planktonic foraminifera. In *Proceedings of the Ocean Drilling Program, Scientific Results* (eds WL Prell, N Niitsuma, KC Emeis, ZK Al-Sulaiman, ANK Al-Tobbah, DM Anderson, RO Barnes, RA Bilak, J Bloemendal, CJ Bray, WH Busch, SC Clemens, P de Menocal, P Debrabant, A Hayashida, JOR Hermelin, RD Jarrad, LA Krissek, D Kroon, DW Murray, CA Nigrini, TF Pedersen, W Ricken, GB Shimmield, SA Spaulding, T Takayama, HL Haven and

- GP Weedon), pp. 257–264. College Station TX: International Ocean Discovery Program.
- Li Y, Clift PD, Böning P, Blusztajn J, Murray RW, Ireland T, Pahnke K and Giosan L (2018) Continuous signal propagation in the Indus submarine canyon since the last deglacial. *Marine Geology* **406**, 159–176.
- Li Y, Clift PD and O'Sullivan PB (2019) Millennial and centennial variations in zircon U-Pb ages in the Quaternary Indus Submarine Canyon. *Basin Research* **31**, 155–70.
- Licht A, Van Cappelle M, Abels HA, Ladant JB, Trabucho-Alexandre J, France-Lanord C, Donnadiu Y, Vandenberghe J, Rigaudier T, Lécuyer C, Terry D Jr, Adriaens R, Boura A, Guo Z, Soe AN, Quade J, Dupont-Nivet G and Jaeger JJ (2014) Asian monsoons in a late Eocene greenhouse world. *Nature* **513**, 501–6.
- Lisiecki LE and Raymo ME (2005) A Pliocene-Pleistocene stack of 57 globally distributed benthic  $\delta^{18}\text{O}$  records. *Paleoceanography* **20**, PA1003.
- Liu R, Lu H, Wang Y, Yu Z, Xu Z, Feng H and Hu R (2018) Grain size analysis of a depositional sequence in the Laxmi basin (IODP hole U1456A, Arabian Sea) reveals the Indian monsoon shift at the mid-Pleistocene climatic transition. *Quaternary Sciences* **38**(5), 1120–1129.
- Long S, McQuarrie N, Tobgay T and Grujic D (2011) Geometry and crustal shortening of the Himalayan fold-thrust belt, eastern and central Bhutan. *Geological Society of America Bulletin* **123**, 1427–47.
- Lu H, Chang H, Guo Z and Zhang P (2015) Continental collision, Qinghai-Tibetan Plateau growth and climate evolution—An introduction to Professor Peter Molnar's scientific contribution. *Scientia Sinica Terrae* **45**, 770–9.
- Lu H, Wang X, An Z, Miao X, Zhu R, Ma H, Li Z, Tan H and Wang X (2004) Geomorphologic evidence of phased uplift of the northeastern Qinghai-Tibet Plateau since 14 million years ago. *Science in China (Series D)* **34**, 855–64.
- Lu H, Zhang H, Wang Y, Zhao L, Wang H, Sun W and Zhang H (2018) Cenozoic depositional sequence in the Weihe Basin (Central China): a long-term record of Asian monsoon precipitation from the greenhouse to icehouse Earth. *Quaternary Sciences* **38**, 1057–67 (in Chinese with English abstract), doi: [10.11928/j.issn.1001-7410.2018.05.01](https://doi.org/10.11928/j.issn.1001-7410.2018.05.01).
- Mahar GA and Zaigham NA (2014). Examining spatio-temporal change detection in the Indus River Delta with the help of satellite data. *Arabian Journal for Science and Engineering* **40**, 1933–46.
- Mehra OP and Jackson ML (1960) Iron oxide removal from soils and clays by a dithionite–citrate system buffered with sodium bicarbonate. In *Proceedings of 7th National Conference on Clays and Clay Minerals*, pp. 317–327. Washington: National Academy of Sciences.
- Meyer I, Davies GR and Stuut J-BW (2011) Grain size control on Sr-Nd isotope provenance studies and impact on paleoclimate reconstructions: an example from deep-sea sediments offshore NW Africa. *Geochemistry, Geophysics, Geosystems* **12**, Q03005.
- Mishra R, Pandey DK, Ramesh P and Clift PD (2016) Identification of new deep-sea sinuous channels in the eastern Arabian Sea. *SpringerPlus* **5**(1), 844–62.
- Mishra R, Pandey DK, Ramesh P and Shipboard Scientific Party SK-306 (2015) Active channel system in the middle Indus fan: results from high-resolution bathymetry surveys. *Current Science* **108**(3), 409–12.
- Molnar P (2001) Climate change, flooding in arid environments, and erosion rates. *Geology* **29**, 1071–5.
- Molnar P, England P and Martinod J (1993) Mantle dynamics, uplift of the Tibetan Plateau, and the Indian monsoon. *Reviews of Geophysics* **31**, 357–96.
- Pandey DK, Clift PD, Kulhanek DK and The Expedition 355 Scientists (2016a) Arabian Sea Monsoon. In *Proceedings of the International Ocean Discovery Program* (eds DK Pandey, PD Clift, DK Kulhanek and The Expedition 355 Scientists). College Station, TX: International Ocean Discovery Program.
- Pandey DK, Clift PD, Kulhanek DK, Andò S, Bendle JAP, Bratenkov S, Griffith EM, Gurumurthy GP, Hahn A, Iwai M, Khim B-K, Kumar A, Kumar AG, Liddy HM, Lu H, Lyle MW, Mishra R, Radhakrishna T, Routledge CM, Saraswat R, Saxena R, Scardia G, Sharma GK, Singh AD, Steinke S, Suzuki K, Tauxe L, Tiwari M, Xu Z and Yu Z (2015) *Expedition 355 Preliminary Report: Arabian Sea Monsoon*. College Station TX: International Ocean Discovery Program.
- Pandey DK, Clift PD, Kulhanek DK, Andò S, Bendle JAP, Bratenkov S, Griffith EM, Gurumurthy GP, Hahn A, Iwai M, Khim B-K, Kumar A, Kumar AG, Liddy HM, Lu H, Lyle MW, Mishra R, Radhakrishna T, Routledge CM, Saraswat R, Saxena R, Scardia G, Sharma GK, Singh AD, Steinke S, Suzuki K, Tauxe L, Tiwari M, Xu Z and Yu Z (2016b) Site U1456. In *Arabian Sea Monsoon*. In *Proceedings of the International Ocean Discovery Program*, 355 (eds DK Pandey, PD Clift, DK Kulhanek and the Expedition 355 Scientists). College Station TX: International Ocean Discovery Program.
- Pearce NJG, Perkins WT, Westgate JA, Gorton MP, Jackson SE, Neal CR and Chenery SP (1997) A compilation of new and published major and trace element data for NIST SRM 610 and NIST SRM 612 glass reference materials. *Geostandards and Geoanalytical Research* **21**, 115–44.
- Prell WL and Kutzbach JE (1987) Monsoon variability over the past 150,000 years. *Journal of Geophysical Research* **92**, 8411–25.
- Prell WL, Murray DW, Clemens SC and Anderson DM (1992) Evolution and variability of the Indian Ocean summer monsoon: evidence from the western Arabian Sea Drilling Program. In *Synthesis of Results from Scientific Drilling in the Indian Ocean* (eds Duncan RA, Rea DK, Kidd RB, von Rad U and Weissel JK), pp. 447–469. Washington DC: American Geophysical Union.
- Prins MA, Postma G, Cleveringa J, Cramp A and Kenyon NH (2000) Controls on terrigenous sediment supply to the Arabian Sea during the late Quaternary: the Indus Fan. *Marine Geology* **169**, 327–49.
- Ren JS (2013) The 1:5 000 000 International Geological Map of Asia (IGMA5000). *Acta Geologica Sinica* **87**(5), 1474.
- Roe GH, Ding Q, Battisti DS, Molnar P, Clark MK and Garzzone CN (2016) A modeling study of the response of Asian summertime climate to the largest geologic forcings of the past 50 Ma. *Journal of Geophysical Research* **121**, 5453–70.
- Scheinost AC (1998) Use and limitations of second-derivative diffuse reflectance spectroscopy in the visible to near-infrared range to identify and quantify Fe oxide minerals in soils. *Clays and Clay Minerals* **46**, 528–36.
- Schildgen TF, Van Der Beek PA, Sinclair HD and Thiede RC (2018) Spatial correlation bias in late-Cenozoic erosion histories derived from thermochronology. *Nature* **559**, 89–93.
- Thiede RC, Arrowsmith JR, Bookhagen B, McWilliams MO, Sobel ER and Strecker M R (2005) From tectonically to erosionally controlled development of the Himalayan orogen. *Geology* **33**, 689–92.
- Thiede RC, Bookhagen B, Arrowsmith JR, Sobel ER and Strecker MR (2004) Climatic control on rapid exhumation along the Southern Himalayan Front. *Earth and Planetary Science Letters* **222**, 791–806.
- Thiede RC and Ehlers TA (2013) Large spatial and temporal variations in Himalayan denudation. *Earth and Planetary Science Letters* **371–372**, 278–93.
- Valdes PJ, Ding L, Farnsworth A, Spicer RA, Li SH and Su T (2019) Comment on “Revised paleoaltimetry data show low Tibetan Plateau elevation during the Eocene”. *Science* **365**(6459), eaax8474, doi: [10.1126/science.aax8474](https://doi.org/10.1126/science.aax8474).
- Vermeesch P (2004) How many grains are needed for a provenance study? *Earth and Planetary Science Letters* **224**, 441–51.
- Wang P, Wang B, Cheng H, Fasullo J, Guo Z, Kiefer T and Liu Z (2017) The global monsoon across time scales: mechanisms and outstanding issues. *Earth-Science Review* **174**, 84–121.
- Yin A (2006) Cenozoic tectonic evolution of the Himalayan orogen as constrained by along-strike variation of structural geometry, exhumation history, and foreland sedimentation. *Earth-Science Reviews* **76**, 1–131.
- Yu Z, Colin C, Wan S, Saraswat R, Song L, Xu Z, Clift P, Lu H, Lyle M, Kulhanek D, Hahn A, Tiwari M, Mishra R, Miska S and Kumar A



- (2019) Sea level-controlled sediment transport to the eastern Arabian Sea over the past 600 kyr: Clay minerals and SrNd isotopic evidence from IODP Site U1457. *Quaternary Science Reviews* **205**, 22–34.
- Zhang H, Lu H, Stevens T, Feng H, Fu Y, Geng J and Wang H** (2018) Expansion of dust provenance and aridification of Asia since ~7.2 Ma revealed by detrital zircon U-Pb dating. *Geophysical Research Letters* **45**, 13437–48.
- Zhang H, Lu H, Xu X, Liu X, Yang T, Stevens T, Bird A, Xu Z, Zhang T, Lei F and Feng H** (2016) Quantitative estimation of the contribution of dust sources to Chinese loess using detrital zircon U-Pb age patterns. *Journal of Geophysical Research: Earth Surface* **121**, 2085–99.
- Zhang P, Molnar P and Downs WR** (2001) Increased sedimentation rates and grain sizes 2–4 Myr ago due to the influence of climate change on erosion rates. *Nature* **410**, 891–7.
- Zhang W, Chen J and Li G** (2015) Shifting material source of Chinese loess since ~2.7 Ma reflected by Sr isotopic composition. *Scientific Reports* **5**, 10235.
- Zhang Y, Ji J, Balsam WL, Liu L and Chen J** (2007) High resolution hematite and goethite records from ODP 1143, South China Sea: Co-evolution of monsoonal precipitation and El Niño over the past 600,000 years. *Earth and Planetary Science Letters* **264**, 136–50.